IEEE Access
Multidisciplinary | Rapid Review | Open Access Journal

Received October 16, 2018, accepted November 22, 2018, date of publication December 7, 2018,
date of current version January 11, 2019.

Digital Object Identifier 10.1109/ACCESS.2018.2885597

Optimal Periodic Control of Hypersonic Cruise Vehicle: Trajectory Features

WENKAI WANG[1], ZHONGXI HOU[1], SHANGQIU SHAN[2], AND LILI CHEN[1]
[1]College of Aerospace Science and Engineering, National University of Defense Technology, Changsha 410073, China
[2]Department of Aerospace Science and Technology, Space Engineering University, Beijing 101400, China

Corresponding author: Zhongxi Hou (hzx@nudt.edu.cn)

This work was supported by the National Natural Foundation of China under Grant 61803383.

ABSTRACT Optimal periodic control is an effective technique to reduce aerodynamic heating and fuel consumption of hypersonic cruise vehicles. Herein, this optimal control problem has been solved by nonlinear programming and passed the posteriori check of optimality. The results indicate that the lift coefficient and velocity in dynamical model could be recognized as constants. Accordingly, the original 3D system consists of velocity, flight path angle, and altitude, which could be decoupled into a 2D subsystem and a 1D one. The 2D subsystem could describe the correlation between the flight path angle and altitude. And the period length is mainly dependent on the maximum altitude difference. The 1D subsystem has been proved to be feasible to describe the variation of kinetic energy or velocity. On basis of the subsystems, the heating and fuel performances of periodic cruise have been studied. The heating performance is mainly dependent on the maximum altitude difference, and the fuel consumption is mainly dependent on the drag coefficient. The features concluded in this paper can support rapid trajectory planning or suboptimal feedback design of hypersonic cruise vehicles.

INDEX TERMS Optimal periodic control, hypersonic cruise vehicle, trajectory features, performances.

I. INTRODUCTION

Hypersonic cruise vehicle (HCV) is a kind of aerial vehicle that cruises at Ma 5 and altitude beyond 20 km. Its high speed is helpful to shorten endurance, especially that of long-range flights. This advantage facilitates the research of hypersonic airliners such as LAPCAT [1], HIKARI [2], and HEXAFLY-Int [3], [4]. Besides, the high speed also endows hypersonic missiles like Boeing X-51A [5], [6] with high penetration ability [7], which is desirable in military [8].

However, speed beyond Mach 5 would induce severe aerodynamic heating on surfaces [9]. To withstand the aerothermodynamics over a long range, a comprehensive and complicated thermal protection/management system is demanded [10], [11]. This would lead to a higher empty ratio, which means decline of structural efficiency [12]. To obtain a long range, lightweight materials for thermal protection is a research hotspot at present [13].

Besides, optimal control has been proven another effective approach [14]–[16]. In works minimizing fuel consumption [7], [17], [18], optimal periodic control is shown also efficient to alleviate aerodynamic heating. Altitude, flight path angle, and velocity of the resultant trajectories behave periodicity during cruise segment. Hence the manner of cruise is called periodic hypersonic cruise (PHC). From perspective of Pines [19], the excellent global reach and heat load performances of PHC are due to a flight regime where the coupled propulsion, aerodynamics and flight physics are simply more efficient. By heat load and specific fuel consumption being optimized together, Kang *et al.* [20] figured out that heat load and fuel consumption could be simultaneously diminished by PHC, and that the two performances mutually conflict. Herein, the adopted models of HCV is referred from our previous work [21]. By minimizing the weighted combination of fuel and heating performances, the results show that PHC is effective to reduce mean heating flux, and that it maintains the similar performance of fuel consumption with steady cruise. The difference between [21] and the other works is the effectiveness of PHC to conserve fuel. This difference is mainly caused by the differences of propulsive and aerodynamic models, which has also been observed by Menon *et al.* [22].

However, as a locally optimizing periodic solution of a Hamiltonian system, PHC is more likely to be unstable, according to Evans's work [23]. The poor stability would lead to failure in realization. Hence more efforts should be made to improve stability and feasibility of PHC. That means

a compromise in optimality. Before such a compromise, a tractable method to construct suboptimal trajectories with improved performances are still significant. To build this method, the mechanism of periodicity, the merit of control to realize periodic cruise, the variation scales of the flight states, the predominant factors deciding fuel and heating performances are necessary to make clear.

The mechanism of PHC to conserve fuel and alleviate heating has been preliminarily analyzed in our previous work [24]. Period length is also included. Although the concluded features are in accord with those of PHC, the rationality of assumptions used in simplification of dynamical system are questionable. Therefore, a further study is necessary.

In this work, the studied features include constant lift coefficient, constant velocity, periodicity, energy cycle, fuel and heating performance. Among these features, constant lift coefficient and constant velocity are used to simplify the problem and make the dynamical system more tractable. Features of periodicity and energy cycle are used to generate temporal arrays of state variables by algebraic correlations. Features of fuel and heating performance are used to estimate the performances of a PHC trajectory. With fuel and heating performances specified, a periodic hypersonic cruise trajectory could be constructed in a procedure as follows:

1) specify the planform loading and the boundaries of control inputs;
2) solve the reference velocity and altitude by optimal steady cruise;
3) estimate the maximum altitude difference and drag coefficient by features of performances;
4) obtain the temporal arrays of velocity, flight path angle, and altitude.

In Section II, the optimal periodic control problem is formulated. The simulation results are exhibited. The control law of thrust coefficient is bang-singular-bang; and that of lift coefficient is likely to be discontinuous. These features have been verified by a posteriori check of necessary conditions derived from Pontryagin's minimum principle. In Section III, the distribution of distance knots is studied. The vehicle spends most of the time/distance at high altitude (or low atmospheric density). By supposing that lift coefficient maintains constant over the whole period, the fuel and heating performances of the simplified system are closed to those of the original system. The optimal lift coefficient (optimized as a parameter) is higher than that related to the maximum L/D. Due to the hypersonic speed, the relative variation of velocity and its impact on variation of flight path angle are negligible. Hence the dynamical models of flight path angle and altitude are decoupled from that of velocity (or specific kinetic energy). The original 3D system is divided into two subsystems: a 2D autonomous subsystem composed by density and flight path angle, and an 1D subsystem of kinetic energy. In Section IV, the features and performances of the PHC are studied. The 2D and 1D subsystems are proved to be feasible to approximate the variations of the state variables governed by the original 3D dynamical system.

TABLE 1. Definition of variables and parameters.

Name	Symbol	Unit	Normalization
Time	t	s	$\tau = t/\sqrt{R_E/g}$
Distance	x	m	$\chi = x/R_E$
Velocity	V	m/s	$u = V/\sqrt{R_E g}$
Specific kinetic energy	K	J/kg	$k = K/(R_E g) = u^2/2$
Flight path angle	γ	-	-
Altitude	H	m	$h = H/R_E$
Atmospheric density	ρ	kg/m^3	$d = \rho/\rho_0$
Planform loading	W_0/S	N/m^2	$\sigma = (R_E\rho_0)/(2m_0/S)$
Specific impulse	I_{sp}	s	$i_{sp} = I_{sp}/\sqrt{R_E/g}$
Fuel mass	m_F	kg	$\mu = m_F/m_0$
Specific combustion enthalpy	H_p	J/kg	$h_p = H_p/(R_E g)$

On basis of the 2D autonomous subsystem, the periodicity is predominantly decided by the natural oscillation of the 2D subsystem. And the period length could be estimated by the maximum altitude difference (a description of oscillation amplitude of altitude history). The mean heat flux could be estimated by the maximum altitude difference. The excellent heating performance is a nature of PHC. The fuel consumption is mainly dependent on the drag coefficient.

II. PERIODIC HYPERSONIC CRUISE TRAJECTORY

A. PROBLEM FORMULATION

Longitudinal phugoid motion of HCV is governed by a nonlinear dynamical system as follows: [20]

$$\begin{cases} \dfrac{\mathrm{d}V}{\mathrm{d}t} = \dfrac{\rho V^2}{2m_0/S}(C_T\cos\alpha - C_D) - \left(g - \dfrac{V^2}{R_E+H}\right)\sin\gamma \\ \dfrac{\mathrm{d}\gamma}{\mathrm{d}t} = \dfrac{\rho V}{2m_0/S}(C_T\sin\alpha + C_L) - \left(g - \dfrac{V^2}{R_E+H}\right)\dfrac{\cos\gamma}{V} \\ \dfrac{\mathrm{d}H}{\mathrm{d}t} = V\sin\gamma \\ \dfrac{\mathrm{d}x}{\mathrm{d}t} = V\cos\gamma. \end{cases} \tag{1}$$

Wherein, the variables and parameters are defined and normalized in Table. 1. $R_E = 6370$ km is the earth radius, $g = 9.8$ m/s^2 is the gravitational acceleration, ρ_0 is the atmospheric density at a reference normalized altitude h_0. In near space ($H =$ 20-100 km), the normalized density could be approximated as an exponent function of the normalized altitude, as shown in (2); where, β is the fitted constant. Besides, C_L, C_D, and C_T are respectively lift, drag, and thrust coefficients. A modified HL-20 lifting-body model [20] is adopted here. In this model, C_D is in a quadratic correlation with C_L, as shown in (3). C_{D0} and K_D are decided by Mach number (or kinetic energy), as shown in (4) and (5). Mach number is another normalization of velocity, as shown in (6); where, V_a is the sound speed which is decided by atmospheric temperature.

$$d = \exp\left[-\beta R_E(h - h_0)\right] \tag{2}$$

$$C_D = C_{D0}(Ma) + K_D(Ma)C_L^2 \tag{3}$$

$$C_{D0} = 0.07115\exp(-0.8061Ma) + 0.007839 \tag{4}$$

$$K_D = 1.85[1 - \exp(-0.2356Ma)] \tag{5}$$

$$Ma = \frac{V}{V_a} \tag{6}$$

With the other three equations in (1) divided by variation ratio of distance $\mathrm{d}x/\mathrm{d}t$, the dynamical system could be converted into a 3D one with respect to distance. Besides, with the following assumptions adopted, the dynamical system could be simplified as (7).

1) γ is a small angle, hence $\tan\gamma \approx \gamma$ and $\cos\gamma \approx 1$;
2) Because of an aerodynamic constraint of stall and a propulsive constraint of scramjet working condition, angle of attack is limited. In this work, the thrust is assumed to be parallel to velocity. The impact of the deflection of thrust on flight path angle is ignored.
3) Since $H \ll R_E$ holds for an airbreathing cruise, the impact of altitude on centrifugal force is ignored.

$$\begin{cases} \dfrac{\mathrm{d}V}{\mathrm{d}x} = \dfrac{\rho V}{2m_0/S}(C_T - C_D) - \left(g - \dfrac{V^2}{R_E}\right)\dfrac{\gamma}{V} \\ \dfrac{\mathrm{d}\gamma}{\mathrm{d}x} = \dfrac{\rho V}{2m_0/S}C_L - \left(g - \dfrac{V^2}{R_E}\right)\dfrac{1}{V^2} \\ \dfrac{\mathrm{d}H}{\mathrm{d}x} = \gamma \end{cases} \tag{7}$$

With the two sides of the variation ratio of velocity with respect to distance in (7) multiplied by V, the variation ratio could be revised as (8).

$$\frac{V\mathrm{d}V}{\mathrm{d}x} = \frac{\rho V^2}{2m_0/S}(C_T - C_D) - \left(g - \frac{V^2}{R_E}\right)\gamma \tag{8}$$

The specific kinetic energy is defined by

$$K = \frac{1}{2}V^2 \tag{9}$$

With specific kinetic energy in (9) and normalizations in Table. 1 substituted into variation ratio in (8), the dynamical model of normalized specific kinetic energy could be formulated as

$$\frac{\mathrm{d}k}{\mathrm{d}\chi} = 2\sigma k d(C_T - C_D) - (1-2k)\gamma \tag{10}$$

With the normalizations in Table. 1 and the definition of specific kinetic energy in (9) substituted into dynamical models of flight path angle and altitude in (7), the dynamical models could be revised as normalized ones. With the two normalized models combined with the one of normalized kinetic energy in (10), a 3D normalized dynamical system with respect to normalized distance could be composed, as shown in (11).

$$\begin{cases} \dot{k} = \dfrac{\mathrm{d}k}{\mathrm{d}\chi} = 2k\cdot\sigma d\,(C_T - C_D) - (1-2k)\gamma \\ \dot{\gamma} = \dfrac{\mathrm{d}\gamma}{\mathrm{d}\chi} = \sigma d C_L - \left(\dfrac{1}{2k} - 1\right) \\ \dot{h} = \dfrac{\mathrm{d}h}{\mathrm{d}\chi} = \gamma. \end{cases} \tag{11}$$

Generally, the control input of a vehicle consists of deflections of control surfaces and throttle of engine. Lift coefficient is dependent on Mach number and angle of attack; thrust coefficient is dependent on throttle, Mach number, and angle of attack. (The detailed models are shown in [20]) Angle of attack is the difference between pitch angle and flight path angle. The former is second integral of angular acceleration which is directly related to the deflections of control surfaces. Since the dynamics of attitude is not explicit contained in the dynamical system in (1), angle of attack could be recognized as an independent variable which realized in attitude control. Hence control input of the dynamical system in (1) could consist of throttle and angle of attack. Since angle of attack and throttle are only explicitly contained in models of thrust and lift coefficients, the impacts of a set of throttle and angle of attack could be equivalent to that of a set of thrust and lift coefficients. And for a given Mach number, throttle and angle of attack could be solved according to thrust and lift coefficients. Therefore, the control input could also consist of thrust and lift coefficients. Let $\mathbf{X}$ and $\mathbf{U}$ respectively denote the state and control vector, as shown in (12).

$$\begin{cases} \mathbf{X} = [k\ \gamma\ h]^{\mathrm{T}} \\ \mathbf{U} = [C_T\ C_L]^{\mathrm{T}} \end{cases} \tag{12}$$

Fuel consumption and aerothermodynamic performance are concerned about in this work. The consumption ratio of fuel mass is governed by (13) [20]. m_F denotes the consumed fuel mass, T_E does the thrust of engine, and I_{sp} does the specific impulse.

$$\frac{\mathrm{d}m_F}{\mathrm{d}t} = \frac{T_E}{gI_{sp}} = \frac{\frac{1}{2}\rho V^2 S C_T}{gI_{sp}} \tag{13}$$

Specific impulse of scramjets could be estimated by (14) [25]. η_{KE} and η_C are respectively kinetic and combustion efficiency. For a hydrocarbon-fueled scramjet, $\eta_{KE} = 0.8$ and $\eta_C = 0.7$ are rational performances. C_C is nondimensional heat of combustion to unit mass of air, C_F is nondimensional fuel enthalpy at the injector manifold to unit mass of air.

$$I_{sp} = \frac{V}{gf}\left[\sqrt{(1+f)\,\eta_{KE}\left(1 + \frac{C_F + \eta_C C_C}{1+\kappa}\right)} - 1\right] \tag{14}$$

Propulsive efficiency is the ratio of useful work done by thrust to chemical energy of fuel, as shown in (15). Hence it is in proportional correlation with velocity and specific impulse. H_p is the specific combustion enthalpy of fuel. For Jet-A, it is about 43.5 MJ/kg; for liquid hydrogen, it is about 119.9 MJ/kg. Herein, a scramjet fueled by Jet-A is adopted.

$$\eta_P = \frac{T_E V}{\dfrac{\mathrm{d}m}{\mathrm{d}t}H_p} = \frac{V I_{sp} g}{H_p} \tag{15}$$

With the two sides of (13) divided by variation ratio of distance $\mathrm{d}x/\mathrm{d}t$ in (1), the variation of fuel mass with respect to distance could be obtained. With (14), (15) and the normalizations in Table. 1 substituted, the dynamical model of fuel mass fraction with respect to normalized time could be formulated as (16).

$$\dot{\mu} = \frac{\sigma d u C_T}{i_{sp}} = \frac{2k\cdot\sigma d C_T}{u i_{sp}} = \frac{2k\cdot\sigma d C_T}{h_p \eta_P} \tag{16}$$

The aerodynamic heat flux at the stagnation point could be estimated by (17) [20]. It is the variation ratio of the heat convected from atmosphere to the vehicle. Q denotes the aerodynamic heat. The heat flux is related to atmospheric density and velocity. k_{q0} is a constant related to bluntness of leading edge [26].

$$q_w = \frac{\mathrm{d}Q}{\mathrm{d}t} = k_{q0}\sqrt{\rho}V^3 \tag{17}$$

With (17) divided by the variation ratio of distance $\mathrm{d}x/\mathrm{d}t$ in (1), and with the normalizations in Table. 1 substituted, the dynamical model of aerodynamic heat could be formulated as (18).

$$\dot{Q} = k_q\sqrt{d}\cdot k \tag{18}$$

In pursuit of high fuel efficiency and low aerodynamic heating, the period-average criterion in (19) is to minimize in optimal control. ω is the weight factor of aerodynamic heating. When a weight factor of 0 is adopted, the problem would become a fuel-optimal one.

$$\min:\ J = \frac{1}{T_\chi}\int_0^{T_\chi}\left(\frac{\dot{\mu}}{\dot{\mu}_0} + \omega\frac{\dot{Q}}{\dot{Q}_0}\right)d\chi \tag{19}$$

Trajectory of the optimal periodic control is a closed orbit in state space $\mathbf{X} = [k\ \gamma\ h]^{\mathrm{T}}$. The trajectory has no terminal points in actual. However, to apply discretization and numerical simulation, initial and final points exist. The initial and final points should coincide to enclose the orbit, as shown in (20). To avoid multiple solutions caused by different initial points on the same closed orbit, one dimension of the initial point could be specified, as shown in (21). The physical significance of this initial point is the lowest altitude. The selection of initial points is without loss of generality.

$$\mathbf{X}(0) = \mathbf{X}(T_\chi) \tag{20}$$

$$\gamma(0) = 0, \quad h < h_0 \tag{21}$$

The limitations of state variables and admissible controls are as follows:

$$\phi(\mathbf{X}) = \begin{bmatrix} k - k_{\min} \\ k_{\max} - k \end{bmatrix} \geq 0 \tag{22}$$

$$\zeta(\mathbf{U}) = \begin{bmatrix} C_T - C_{T\min} \\ C_{T\max} - C_T \\ C_L - C_{L\min} \\ C_{L\max} - C_L \end{bmatrix} \geq 0 \tag{23}$$

B. REFERENCE TRAJECTORY: OPTIMAL STEADY CRUISE

To study the advantages of PHC over steady cruise, an optimal steady cruise is used as the reference trajectory [27]. As an equilibrium point of dynamical system shown in (11), steady cruise should satisfy the condition shown in (24). This condition means that the vehicle cruises at constant velocity and altitude.

$$\begin{cases} k = k_0 \\ \gamma \equiv 0 \\ h = h_0 \Rightarrow d_0 = 1 \end{cases} \tag{24}$$

With this condition substituted into the dynamical system in (11), the control inputs, namely thrust and lift coefficients, could be expressed as functions of velocity and altitude, as shown in (25). Then an equilibrium plane $k_0 - h_0$ could be enclosed by the constraints in (22)-(23). Any one point in the plane is a feasible solution to steady cruise. Then the optimal steady cruise could be solved by a parametric optimization in the equilibrium plane.

$$\begin{cases} C_T = C_D \\ C_L = \dfrac{1}{\sigma}\left(\dfrac{1}{2k_0} - 1\right) \end{cases} \tag{25}$$

With the heating performance ignored, the objective is to minimize the fuel consumption, as shown in (26).

$$J_0 = \dot{\mu}_0 = \frac{2k_0\sigma C_T}{h_p\eta_{P0}} \tag{26}$$

In the equilibrium plane, with control inputs in (25) substituted into objective of optimal steady cruise in (26), the objective could be revised as

$$J_0 = \dot{\mu}_0 = \frac{1 - 2k_0}{h_p\eta_{P0}E} \tag{27}$$

According to the objective in (27), to minimize the specific fuel consumption, the maximum L/D related to a given velocity should be adopted. On basis of the aerodynamic model in (3), the maximum L/D could be obtained, as shown in (28). The equation indicates that the maximum L/D is only decided by velocity (or specific kinetic energy).

$$E_{\max} = \frac{1}{2\sqrt{C_{D0}K_D}} \sim k_0 \tag{28}$$

Then the objective could be further revised as a function of velocity, as shown in (29). The values of function ψ related to different Mach numbers are shown in Fig. 1. The figure indicates that ψ declines with increment of Mach number ($Ma \in [4, 6]$). Therefore, Mach 6 is the optimal velocity of steady cruise.

$$J_0 = \dot{\mu}_0 = \frac{1 - 2k_0}{\eta_{P0}h_pE_{\max}} \triangleq \frac{1}{h_p}\psi(k_0) \tag{29}$$

By combining equilibrium condition in (25) and the definition of σ in Table. 1, the optimal density could be solved, as shown in (30); where, C_{Lk} is the lift coefficient related to maximum L/D, as shown in (31). Then the optimal altitude could be obtained by interpolation with the atmospheric data of 1976 Committee on Extension to the Standard Atmosphere (COESA). The optimal altitudes for vehicle with different planform loadings are shown in Fig. 2. For a vehicle with planform loading of 273 kg/m^2, the optimal altitude is 30 km.

$$\rho_0 = \frac{2m_0/S}{R_E C_{Lk}}\left(\frac{1}{2k_0} - 1\right) \tag{30}$$

$$C_{Lk} = \frac{1}{2\sqrt{C_{D0}K_D}} \tag{31}$$

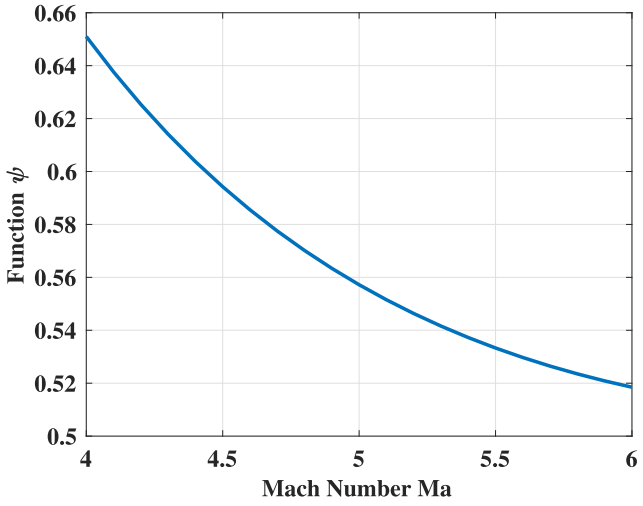

FIGURE 1. Value of function ψ.

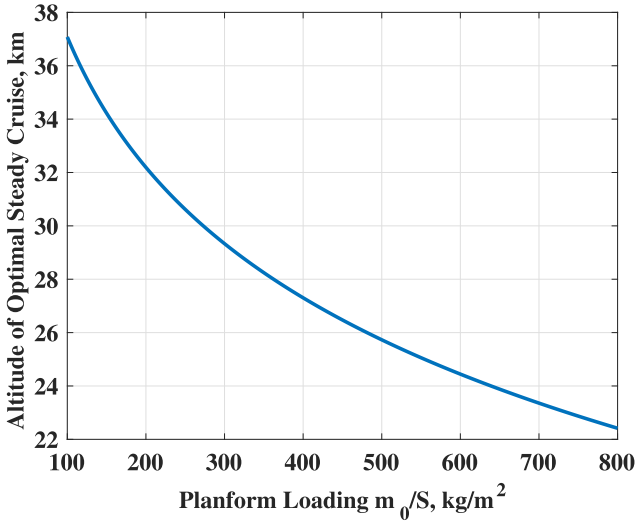

FIGURE 2. Altitudes of optimal steady cruise for HCV with different planform loadings.

Then the heating performance of optimal steady cruise could be obtained, as shown in (32).

$$\dot{Q}_0 = k_q\sqrt{d_0}k_0 = k_q k_0 \tag{32}$$

With this heating performance substituted into (19), the performance measure of optimal periodic cruise could be revised as

$$\min:\ J = \frac{1}{T_\chi}\int_0^{T_\chi} \Phi d\chi \tag{33}$$

where,

$$\Phi = \frac{\dot{\mu}}{J_0} + \omega\sqrt{d}\frac{k}{k_0} \tag{34}$$

In this work, the solution for optimal steady cruise could be summarized as follows:

$$\begin{cases} \mathbf{X}_0 = [k_{\max}, 0, h_0]^{\mathrm{T}} = [0.0260, 0, 0.00471]^{\mathrm{T}} \\ \mathbf{U}_0 = [C_{Lk}, C_D(C_{Lk})]^{\mathrm{T}} = [0.0168, 0.0775]^{\mathrm{T}} \\ J_0 = \dot{\mu}_0 = 0.7441 \end{cases} \tag{35}$$

C. METHOD FOR OPTIMAL CONTROL

The optimal control problem could be expressed as one to optimize the state and control variables shown in (12) and limited by (22) and (23) to maximize the performance measure of (33), while satisfying the boundary conditions in (20) and (21).

The normalized distance χ is uniformly discretized into a series of knots, as shown in (36). N is the number of knots. T_χ is unknown and optimized as a parameter.

$$\chi^{(i)} = (i-1)\cdot\frac{T_\chi}{N-1}, \quad i = 1, 2, \cdots, N \tag{36}$$

At the knots, the state and control variables are also discretized as

$$\begin{cases} \mathbf{X}^{(i)} = [k^{(i)}\ \gamma^{(i)}\ h^{(i)}]^{\mathrm{T}} = [k(\chi^{(i)})\ \gamma(\chi^{(i)})\ h(\chi^{(i)})]^{\mathrm{T}} \\ \mathbf{U}^{(i)} = [C_T^{(i)}\ C_L^{(i)}]^{\mathrm{T}} = [C_T(\chi^{(i)})\ C_L(\chi^{(i)})]^{\mathrm{T}} \end{cases} \tag{37}$$

The differential correlations of dynamical system in (11) are then converted into algebraic equation constraints by numerical integration method. Herein, 2-stage 4-order Gauss-Legendre implicit method [28] based on Gauss quadrature is adopted. For any $i \in [1, N-1]$ and $i \in Z$, in the interval between i-th and $(i+1)$-th knots, there are two additional collocation points. At these points, the control input maintains $\mathbf{U}^{(i)}$. At the j-th ($j = 1, 2$) collocation point in i-th interval, let $\mathbf{K}_j^{(i)}$ denote the gradient of state vector $\mathbf{X}$ with respect to normalized distance χ. For the time-invariant dynamical system in (11), the differential correlation could be converted into 3 equation constraints in one interval, as shown in (38). a_{jl} and b_j are coefficients in Butcher tableau of Gauss-Legendre.

$$\begin{cases} \mathbf{X}^{(i+1)} - \mathbf{X}^{(i)} - \Delta\chi\sum_{j=1}^{2} b_j\mathbf{K}_j^{(i)} = \mathbf{0} \\ \mathbf{K}_j^{(i)} - f\left(\mathbf{X}^{(i)} + \Delta\chi\sum_{l=1}^{2} a_{jl}k_l, \mathbf{U}^{(i)}\right) = \mathbf{0} \end{cases} \tag{38}$$

The problem is solved by a nonlinear programming solver IPOPT [29], the Jacobian and Hessian are provided by an automatic differentiation solver ADOL-C [30].

Simulations with weight factors from 0 to 5.0 in step of 0.1 have been conducted. For weight factor of 0, the result of optimal steady cruise in (35) and $\mathbf{K}_1^{(0)} = \mathbf{K}_2^{(0)} = \mathbf{0}$ is adopted as the initial guess. For weight factors higher than 0, the simulations are conducted sequentially: the result of the previous simulation is used as the initial guess, as shown in (39). Wherein, *Opt* denotes a function describing the solving process of optimal control, i denotes the i-th step with

weight factor ω_i. Weight factor and initial guess for state and control variables are independent variables of Opt.

$$\begin{bmatrix} \mathbf{X}^{(i)} \\ \mathbf{K}_1^{(i)} \\ \mathbf{K}_2^{(i)} \\ \mathbf{U}^{(i)} \end{bmatrix} = Opt\left(\omega_i; \quad \mathbf{X}^{(i-1)}, \mathbf{K}_1^{(i-1)}, \mathbf{K}_2^{(i-1)}, \mathbf{U}^{(i-1)}\right) \tag{39}$$

D. METHOD FOR POSTERIORI CHECK

Evans [23] suggests sufficient and necessary conditions for local minimum of periodic control in four aspects as follows:

1) The Euler-Langrange equations and the transversality conditions must be satisfied;
2) The strong form of the Legendre condition related to the second derivative of Hamiltonian with respect to control input should be positive definite, i.e. $\mathcal{H}_{uu} > 0$;
3) A bounded symmetric solution to the Riccati equation exists for $0 \leq t \leq T$ subject to the periodic boundary condition;
4) Eigenvalues of transition matrix evaluated over one period are unity or off the unit circle.

In this work, the former two conditions are adopted to conduct a rough posteriori check of optimality of the numerical solutions. The latter two demand solving Riccati equation over one period, which means additional numerical analyses. Herein, the latter two are not studied. Besides, Evans [23] has proved that local optimizing periodic solutions are unstable with the possible exception of isolated limit points. To avoid solving Riccati equation, the solutions in this optimal periodic control problem are supposed to be unstable. Hence they could be recognized infeasible. Nevertheless, detailed studies of the optimality, stability, and feasibility are still necessary in the future.

The Hamiltonian of the optimal periodic control problem could be formulated as

$$\mathcal{H} = \Lambda^{\mathrm{T}}\dot{\mathbf{X}} + \Phi \tag{40}$$

where, Λ is vector of costates related to $\mathbf{X}$.

$$\Lambda = [\lambda_k \ \lambda_\gamma \ \lambda_h]^{\mathrm{T}}. \tag{41}$$

Then first-order derivative of Hamiltonian with respect to control input could be obtained as

$$\mathcal{H}_u = \frac{\partial \mathcal{H}}{\partial \mathbf{U}} = \begin{bmatrix} \lambda_k \cdot 2k\sigma d + \dfrac{1}{J_0}\dfrac{2k\sigma d}{\eta_P h_p} \\ -\lambda_k \cdot 2k\sigma d \cdot 2K_D C_L + \lambda_\gamma \cdot \sigma d \end{bmatrix} \tag{42}$$

With constraints in (22) and (23) considered, the Lagrangian of the problem could be obtained, as shown in (43).

$$\mathcal{L} = \mathcal{H} + \tilde{\nu}^T \phi + \tilde{\mu}^T \zeta \tag{43}$$

Wherein, $\tilde{\nu}$ and $\tilde{\mu}$ are adjoint vectors related to respectively ϕ and ζ. To minimize the performance measure in (33), all items in the two vectors are nonpositive, and the conditions in (44) and (45) hold [31].

$$\tilde{\nu}_i \begin{cases} = 0, & \phi_i \neq 0 \\ < 0, & \phi_i = 0, \end{cases} \quad i = 1, 2 \tag{44}$$

$$\tilde{\mu}_i \begin{cases} = 0, & \zeta_i \neq 0 \\ < 0, & \zeta_i = 0, \end{cases} \quad i = 1, 2, 3, 4 \tag{45}$$

According to Pontryagin's minimum principle, the necessary condition for optimality is that the partial derivatives of Lagrangian with respect to control inputs vanish, as shown in (46) and (47).

$$0 = \frac{\partial \mathcal{L}}{\partial C_T} = \frac{\partial \mathcal{H}}{\partial C_T} + \tilde{\mu}_1 - \tilde{\mu}_2 \tag{46}$$

$$0 = \frac{\partial \mathcal{L}}{\partial C_L} = \frac{\partial \mathcal{H}}{\partial C_L} + \tilde{\mu}_3 - \tilde{\mu}_4 \tag{47}$$

According to (46), the optimal thrust coefficient satisfies the following scenes:

1) If $\partial\mathcal{H}/\partial C_T > 0$, $\tilde{\mu}_1$ should be nonzero, hence $C_T = C_{T\min}$ should be adopted.
2) If $\partial\mathcal{H}/\partial C_T < 0$, $\tilde{\mu}_2$ should be nonzero, hence $C_T = C_{T\max}$ should be adopted.
3) If $\partial\mathcal{H}/\partial C_T = 0$, a C_T where ϕ_1 and ϕ_2 are inactive should be adopted. Since C_T is not explicitly contained in $\partial\mathcal{H}/\partial C_T$, the control is singular.

The optimal control law of thrust coefficient could be formulated as

$$C_T = \begin{cases} C_{T\max}, & \Delta_T < 0 \\ C_{T\min}, & \Delta_T > 0 \\ \text{singularity}, & \Delta_T = 0 \end{cases} \tag{48}$$

where, Δ_T is the switching discriminant, as defined in (49). With this discriminant substituted into derivative of Hamiltonian in (42), it could be observed that Δ_T has the same sign with $\partial\mathcal{H}/\partial C_T$.

$$\Delta_T = J_0 \eta_P h_p \lambda_k + 1 \tag{49}$$

Similarly, the optimal control law of lift coefficient could be obtained as

$$C_L = \begin{cases} C_{L\max}, & \Delta_L < 0 \\ C_{L\min}, & \Delta_L > 0 \\ \dfrac{1}{4kK_D} \cdot \dfrac{\lambda_\gamma}{\lambda_k}, & \Delta_L = 0 \end{cases} \tag{50}$$

where, Δ_L is the switching discriminant defined in (51). It has the same sign with $\partial\mathcal{H}/\partial C_L$.

$$\Delta_L = -4\lambda_k k K_D C_L + \lambda_\gamma \tag{51}$$

According to [32], for a control problem with state constraint as

$$\zeta(x(t), t) \geq 0 \tag{52}$$

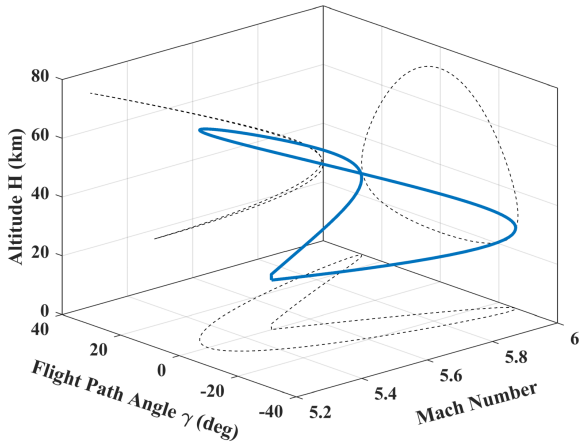

FIGURE 3. Closed orbit of states of optimal PHC ($\omega = 1$).

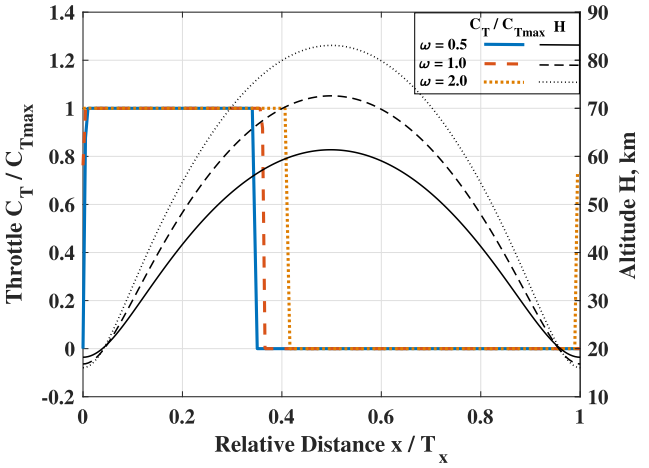

FIGURE 4. Histories of thrust coefficient and altitude of optimal PHC.

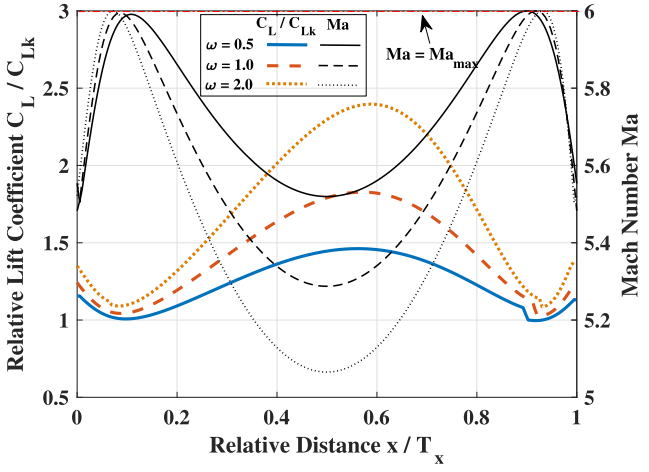

FIGURE 5. Histories of lift coefficient and Mach number of optimal PHC.

at the junction time τ, the boundary interval where $\zeta = 0$ starts or ends. Then the costate of x is likely to be discontinuous at τ, as shown in (53).

$$\lambda(\tau^-) = \lambda(\tau^+) + \eta(\tau)\zeta_x \tag{53}$$

Since state constraints in (23) is only dependent on kinetic energy, history of λ_k may be discontinuous at junction time of $k = k_{\max}$ or $k = k_{\min}$. (50) indicates that control law of lift coefficient is correlative with the costates (or adjust coefficients) of kinetic energy and flight-path angle. Hence the history of lift coefficient may also be discontinuous at the junction time.

Besides, a strong form of the Legrendre condition shown in (54) should be satisfied.

$$\mathcal{H}_{uu} = \frac{\partial^2 \mathcal{H}}{\partial \mathbf{U}^2} = \begin{bmatrix} 0 & 0 \\ 0 & -\lambda_k \cdot 2k\sigma d \cdot 2K_D \end{bmatrix} > 0 \tag{54}$$

The condition is equivalent to

$$\lambda_k < 0 \tag{55}$$

Therefore, as a posteriori check of optimality, the resultant trajectory should satisfy three intuitive aspects as follows:

1) History of thrust coefficient is in a bang-singular-bang form switching between $C_{T\min}$ and $C_{T\max}$.
2) In history of lift coefficient, discontinuity only occurs at the junction time of boundaries $k = k_{\min}$ or $k_{\max}$.
3) History of costate of specific kinetic energy λ_k maintains beneath 0.

E. SIMULATION RESULTS

The optimal periodic hypersonic cruise trajectory with weight factor of 1 is plotted in Fig. 3. The coordination system in the figure is composed by Mach number, flight path angle, and altitude. The trajectory is a closed orbit in state space. Hence the terminal constraint of periodicity in (20) could be satisfied. Besides, the state variables are within the admissible scale.

The histories of thrust coefficient and altitude are plotted together in Fig. 4. The history of thrust coefficient is obviously a bang-bang control switching between boundary arcs $C_T = C_{T\max}$ and $C_T = C_{T\min} = 0$. Besides, the start point of engine is observed to be the minimum altitude. Since the contribution of propulsion to dynamical system in (11) is multiplied by density, whether the engine is working at high altitude has little difference. Hence the trajectory could mainly includes two segments:

1) boosting to ascend;
2) gliding to descend.

The histories of lift coefficient and Mach number are plotted together in Fig. 5. The history of lift coefficient is discontinuous only at the junction points of boundary $Ma = Ma_{\max}$ (equivalent to $k = k_{\max}$).

The history of costate of specific kinetic energy λ_k is plot in Fig. 6. The figure indicates that the history maintains beneath 0 over one period.

Therefore, the histories of state variables satisfy the periodic constraints in (20) and limitations in (22), and that of

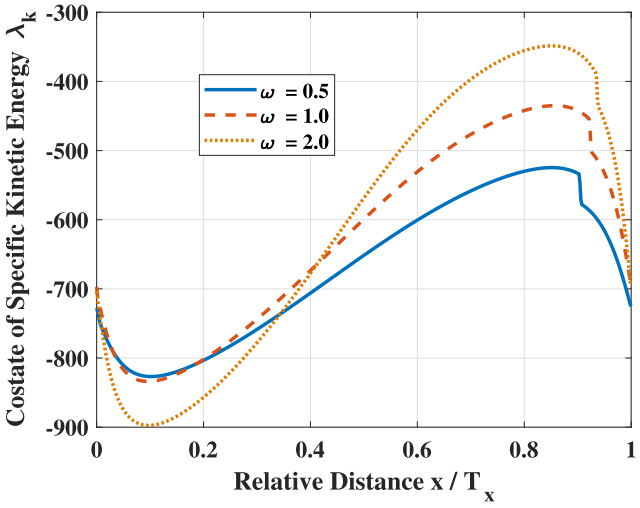

FIGURE 6. History of costate of specific kinetic energy λ_k.

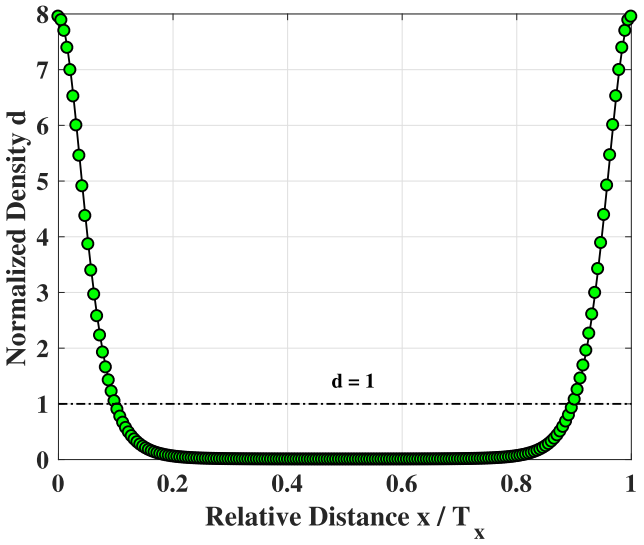

FIGURE 7. Distribution of distance knots in normalized density ($\omega = 1$).

control variables could pass the posteriori check of optimality in Subsection II-D.

III. PROBLEM SIMPLIFICATION AND SYSTEM APPROXIMATION

A. DISTRIBUTION OF DISTANCE KNOTS

On basis of the exponent approximation in (2), the derivative of normalized density with respect to normalized distance could be obtained as

$$\dot{d} = -\beta R_E \cdot d \cdot \dot{h} \tag{56}$$

where, β is the fitted constant of density in (2), R_E is the earth radius. With the two constants involved, a constant ε could be defined, as shown in (57). With data substituted, ε is about 0.001.

$$\varepsilon = \frac{1}{\beta R_E} \approx 0.001 \tag{57}$$

With ε in (57) and $\dot{h}$ in (11) substituted in (56), the variation of normalized density could be revised as

$$\varepsilon \dot{d} = -\gamma d \tag{58}$$

Since $\varepsilon > 0$ and $d > 0$, when $\gamma > 0$, the variation of density is stable, and would converge to $d = 0$; when $\gamma < 0$, density would diverge to $+\infty$. Besides, $\gamma = 0$ is an equilibrium point of the system of density in (58). At this point, let a constant, d_{eq}, denote the normalized density.

When $|\gamma| > \varepsilon$, variation speed of density would be rapid. However, when close to the equilibrium point $\gamma = 0$, γ becomes comparable with ε. The variation of density would slow down. According to dynamical models of altitude and density in (11) and (58), $\gamma = 0$ is simultaneously related to the local extrema of altitude and density. Therefore, the vehicle mainly stays at the locally minimum and maximum altitudes.

Besides, according to the dynamical model of density in (58), for a given flight path angle, a high density would yield a high variation speed of density. Hence the vehicle would stay at the maximum altitude for longer distance than at the minimum. Therefore, most distance knots would be located at low density ($d < 1$).

The distribution of knots in normalized density of PHC with weight factor of 1 is shown in Fig. 7. The abscissa is the relative distance, and the ordinate is the normalized density. On the curve, every circle marker means a distance knot. The knots uniformly divide the distance. The figure validates that the vehicle mainly stays at high altitude with low density.

B. APPROXIMATION OF CONSTANT LIFT COEFFICIENT

With the dynamical model of density in (58) taken derivative with respect to normalized distance, the second-order derivative of normalized density could be obtained as

$$\varepsilon \ddot{d} = -\dot{\gamma} d + \frac{\gamma^2}{\varepsilon} d. \tag{59}$$

With dynamical model of flight path angle in (11) substituted, (59) could be revised as

$$\varepsilon \ddot{d} = -\sigma C_L d^2 + \left(\frac{1}{2k} - 1 + \frac{\gamma^2}{\varepsilon} \right) d \tag{60}$$

A high lift coefficient could help to decrease $\dot{d}$. This is beneficial to the motion towards low density, whereas retards that towards high density. Then more time/distance would be spent at high altitude. Therefore, high lift coefficient is desirable for heat protection. However, around the minimum altitude, the energy loss caused by drag would be considerable if the lift coefficient is too high, which should be avoided to conserve fuel. Therefore, the two parts of criterion in (33) mainly conflict at low altitude. Fig. 5 validates this conclusion in two aspects:

1) when heat protection is more considered, the lift coefficient would be higher, and the main increment occurs at high altitude;
2) at a low altitude, lift coefficient approaches to C_{Lk} which is related to the maximum L/D.

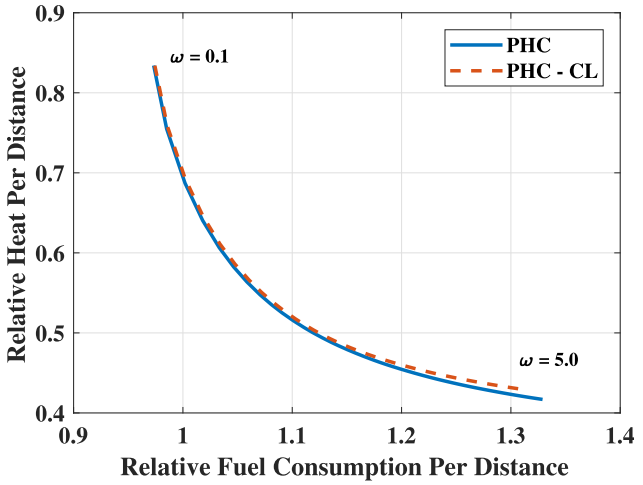

FIGURE 8. Comparison of performances between PHC and PHC-CL trajectories.

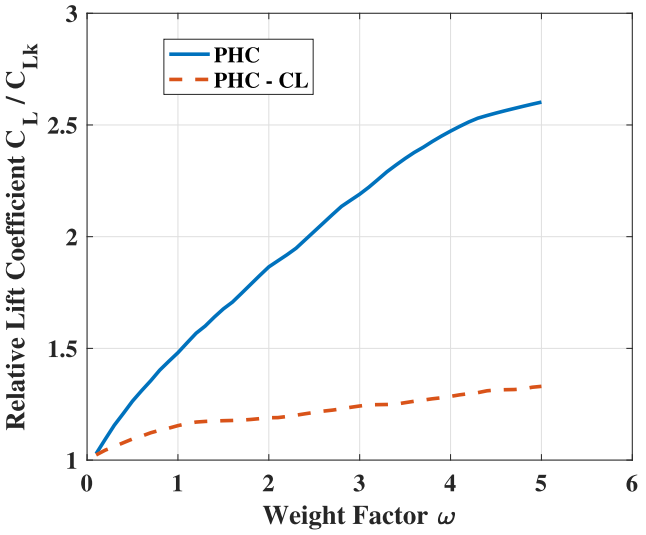

FIGURE 9. Comparison of optimal lift coefficients of PHC-CL and mean values of PHC-CL trajectories.

At high altitude ($d \ll 1$), as shown in dynamical system of (11), a small d would reduce the influence of aerodynamic coefficients. Difference in influences between a certain feasible lift coefficient and the optimal history is ignorable there. However, the influence of difference is considerable at low altitude. Fig. 5 indicates that lift coefficient varies in a small scale at low altitude. A constant lift coefficient close to the mean value at low altitude could diminish the difference. Therefore, it is rational to recognize C_L as a parameter of optimal control that maintains constant along distance/time.

The fuel and heating performances are shown in Fig. 8. In the figure, PHC denotes the result of original optimal control problem, and PHC-CL does that of the problem where lift coefficient is optimized as a parameter. The figure indicates that PHC-CL has similar performances with PHC. The difference is reflected on the weight factors. However, weight factor describes the degree of consideration which is not really a countable quantity. Comparison of weight factors between different systems is insignificant. Therefore, although mismatch between performances and weight factor occurs, PHC-CL is still a rational approximates of PHC.

Besides, the optimal lift coefficients (C_{Lopt}) of PHC-CL are compared with the mean ones ($\bar{C}_L$) of PHC in Fig. 9. The figure shows that a higher weight factor demands a higher lift coefficient in the each of the problems. However, the augment scale of C_{Lopt} is much smaller than that of $\bar{C}_L$. For $\omega \in [0.1, 5]$, C_{Lopt} varies within [1, 1.33].

C. APPROXIMATION OF CONSTANT VELOCITY

Figure. 10 plots the histories of specific mechanical, kinetic, and potential energies. The abscissa, x/T_x, represents the relative distance. x is the distance, and T_x is the period length in distance. The ordinate represents the specific energies in MJ/kg. The figure indicates that mechanical energy conservation approximately holds at most of the distances.

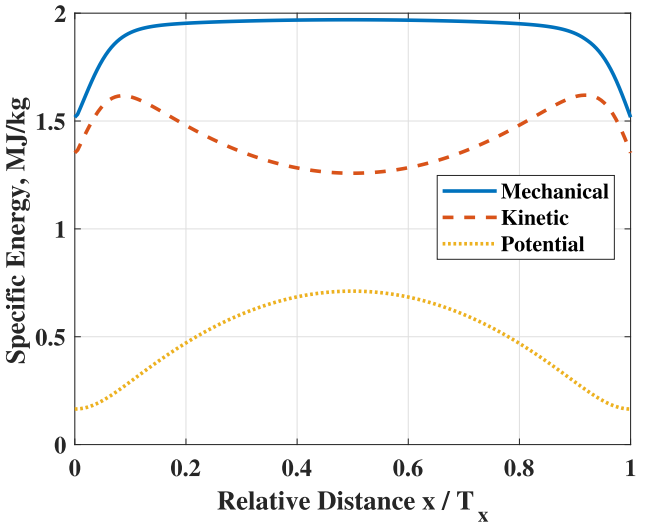

FIGURE 10. Specific energy variation ($\omega = 1$).

The error is small when potential energy is high. Since potential energy is proportional to altitude, the energy conservation mainly holds at high altitude. At high altitude, the density is low, hence energy imported by propulsion and that consumed by drag are negligible. The energy conservation could be formulated as (61). Wherein, gH is the specific potential energy; and $V^2/2$ is the specific kinetic energy.

$$gH + \frac{V^2}{2} = \text{const} \tag{61}$$

With velocity substituted by Mach number in (6), the variations of altitude and Mach number are correlated in the way of (62). For Mach number within 4-6, 1% decrease of Mach number would cause increment of altitude by 1.47-3.31 km. According to (2), this would lead to 20-40 %

decline of density. Therefore, from perspective of energy conversion, small variation of Mach number would lead to prominent variation of altitude or density. According to Fig. 3, to enclose a periodic hypersonic cruise, Mach number only needs a relative variation less than 10%. This is much less prominent than the other state variables. Therefore, variation of velocity (Mach number, or kinetic energy) could be recognized as a small quantity.

$$\frac{\Delta H}{\Delta Ma/Ma} = -\frac{V_a^2}{g} Ma^2 \tag{62}$$

According to dynamical model of flight path angle in (11), a perturbation of kinetic energy, Δk, has an impact on flight path angle as

$$\dot{\gamma} = \sigma d C_L - \left(\frac{1}{2k} - 1\right) + \frac{1}{2k^2}\Delta k \tag{63}$$

Then the error of substituting k by a constant k_0 could be estimated by (64). Normalized kinetic energy of optimal steady cruise in (35) is adopted as k_0.

$$\Delta\dot{\gamma} = \frac{1}{2k_0^2}\Delta k = \frac{1}{k_0}\frac{\Delta Ma}{Ma} \tag{64}$$

For a given relative variation $\Delta Ma/Ma$, the error of ignoring impact of this variation on flight path angle would decline with increment of velocity (Mach number, or kinetic energy). Besides, a low value of $\Delta Ma/Ma$ is possible, according to (62). Therefore, hypersonic speed rationalizes an assumption that impact of variation of velocity (Mach number, or kinetic energy) on dynamical model of flight path angle in (11) is negligible.

D. PROBLEM SIMPLIFICATION

Subsection III-B rationalizes optimizing lift coefficient as a parameter. In dynamical system governed by (11), with a constant lift coefficient, thrust coefficient would be the only control variable, and is only explicitly contained in dynamical model of specific kinetic energy.

Subsection III-C indicates that velocity in dynamical model of flight path angle could be recognized as a constant. With this approximation adopted, the variations of flight path angle and normalized density are coupled; however, independent on velocity.

Then the original 3D dynamical system in (11) could be divided into two subsystems as follows:

1) $d-\gamma$ 2D autonomous subsystem where $k = k_0$ is a constant, and C_L is a constant control input which is optimized as a parameter;
2) 1D subsystem of k, explicitly contains thrust coefficient C_T, and dependent on normalized density d and flight path angle γ.

Load factor is a description of acceleration in lift direction. It is a ratio of lift to weight, as shown in (65).

$$n = \frac{L}{W} = \frac{\sigma d C_L}{1/2k - 1} \tag{65}$$

This equation indicates that load factor is also the ratio between two parts of dynamical model of flight path angle in (11). With (65) substituted, this dynamical model could be revised as

$$\dot{\gamma} = (n-1)\Gamma \tag{66}$$

where, Γ is a constant correlative with k, as defined in (67).

$$\Gamma = \frac{1}{2k} - 1 \tag{67}$$

In the optimal steady cruise, $\gamma \equiv 0$. Hence $n \equiv 1$, which means the lift-weight balance. Then the correlation in (65) could be revised as

$$\sigma d_0 C_{Lk} = \Gamma. \tag{68}$$

With (68) substituted into (65), then the proportional correlation between load factor and normalized density could be figured out as

$$n = \frac{d}{d_0}\frac{C_L}{C_{Lk}} \propto d. \tag{69}$$

With (69) substituted into (58), the dynamical model of load factor could be obtained, as shown in (70).

$$\varepsilon\dot{n} = -n\gamma \tag{70}$$

With load factor in (65) substituted into dynamical model of specific kinetic energy in (11), the dynamical model could be revised as

$$\dot{k} = (1-2k)(nC_A - \gamma) \tag{71}$$

C_A is the open-loop input of combined aerodynamics and propulsion, as defined in (72).

$$C_A = \frac{C_T - C_D}{C_L} \tag{72}$$

Since item in the latter bracket of (71) has a more obvious variation than that in the former one, substituting $k = k_0$ into (71) is also feasible. Hence $(1-2k)$ could be recognized as a constant. For Mach number within 4-6, this item ranges from 0.95 to 0.9, which means it is negligible. Then the dynamical model of specific kinetic energy could be simplified as

$$\dot{k} = nC_A - \gamma \tag{73}$$

Therefore, the $d-\gamma$ 2D subsystem is equivalent to a $n-\gamma$ one governed by (66) and (70), and the k 1D subsystem is governed by (73). The open-loop dynamical system is shown in Fig. 11. In the figure, C_A defined in (72) is the open-loop input, C_L is a constant parameter, $1/s$ means integration process. The figure indicates that the 2D subsystem is autonomous, whereas the 1D subsystem is dependent on C_A and the state variables of the 2D one.

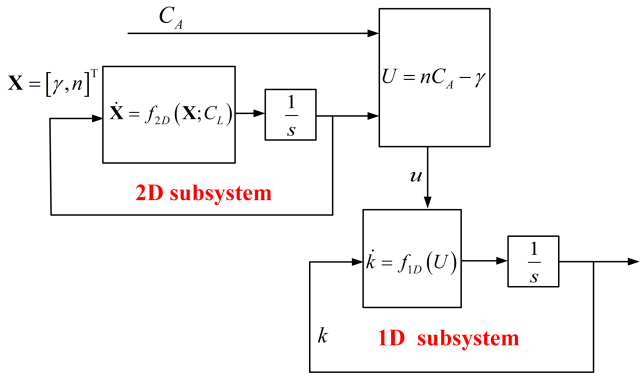

FIGURE 11. Sketch map of simplified open-loop dynamical system.

IV. TRAJECTORY FEATURES

A. PERIODICITY

With $\dot{\gamma}$ in (66) divided by $\dot{n}$ in (70), χ becomes no longer explicitly contained in the 2D $n-\gamma$ subsystem, as shown in (74).

$$\gamma \cdot \mathrm{d}\gamma = \varepsilon\Gamma\left(\frac{1}{n}-1\right)\cdot \mathrm{d}n \tag{74}$$

With the two sides in (74) integrated separately, an algebraic equation could be obtained to describe a closed orbit symmetric about the n axis ($\gamma = 0$), as shown in (75). C is the integration constant.

$$\gamma^2 = 2\varepsilon\Gamma(\ln n - n + C) \tag{75}$$

At the maximum and minimum altitudes, load factor also hits its extrema, and $\gamma = 0$ holds. Hence the integration constant C could be obtained at these extrema, as shown in (76). According to definition of load factor in (65) and exponent estimation of normalized density in (2), $n_{\min}$ is dependent on the maximum altitude difference between the periodic and steady cruise trajectories. The maximum altitude difference is denoted by ΔH. Similarly, $n_{\max}$ is dependent on the minimum altitude difference between the two cruise trajectories, and denoted by $\Delta H_{(\min)}$. Without loss of generality, $n_{\min}$ is used to estimate this integration constant C.

$$C = n_{\min} - \ln n_{\min} = n_{\max} - \ln n_{\max} \geq 1 \tag{76}$$

With the definition of load factor in (65) substituted into the exponent estimation of normalized density, the correlation between altitude difference and load factor could be formulated as

$$\Delta H = -\frac{1}{\beta}\left(\ln n + \ln\frac{C_L}{C_{Lk}}\right). \tag{77}$$

For $C_L/C_{Lk} \in [1, 1.33]$, the maximum altitude difference caused by lift coefficient is -1.81 km. It is a small quantity compared with the practical maximum altitude difference. Hence the impact of lift coefficient could be ignored. And this correlation could be approximated as

$$\Delta H = -\frac{1}{\beta}\ln n. \tag{78}$$

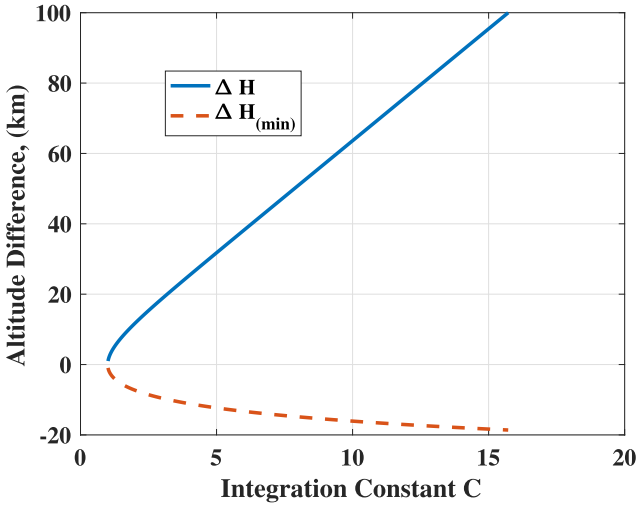

FIGURE 12. Maximum and minimum altitude differences of periodic cruise trajectories.

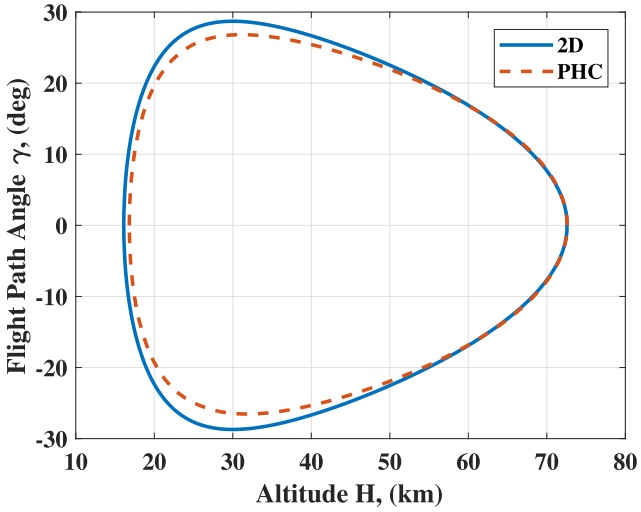

FIGURE 13. $n-\gamma$ phase portraits of the 2D system and PHC ($\omega = 1$).

The maximum and minimum altitude differences at different integration constants are plotted in Fig. 12. The figure indicates that the minimum altitude difference decreases with the increment of the maximum altitude difference. Hence a vehicle which jumps higher would dive lower.

The $n-\gamma$ phase portraits of the 2D subsystem and PHC are compared in Fig. 13. The figure shows that the 2D subsystem approximates PHC well.

With solution of flight path angle in (75) substituted into dynamical model of load factor in (70), the variation ratio of normalized distance with respect to load factor could be figured out, as shown in (79).

$$\frac{\mathrm{d}\chi}{\mathrm{d}n} = \frac{1}{\dot{n}} = -\sqrt{\frac{\varepsilon}{2\Gamma}}\frac{1}{n\sqrt{\ln n - n + C}} \tag{79}$$

Then the integral of (79) from $n_{\max}$ to $n_{\min}$ could suggest half of the period length in normalized distance, as shown

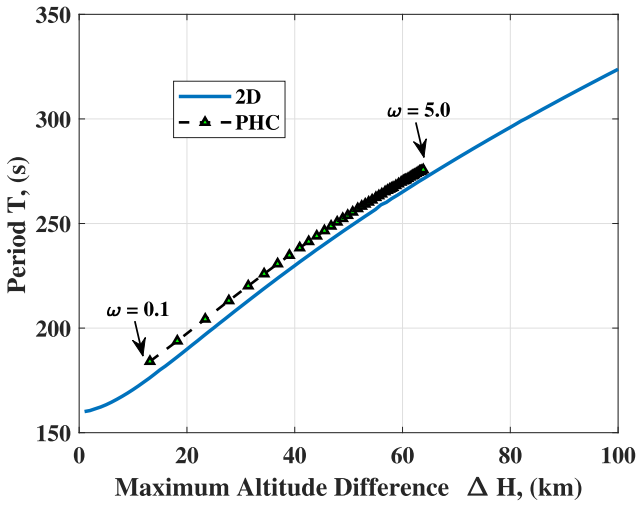

FIGURE 14. Period lengths of PHC and 2D autonomous subsystem.

in (80). The equation indicates that T_χ is inversely proportional to $\sqrt{\Gamma}$.

$$T_\chi = 2\int_{n_{\max}}^{n_{\min}} \frac{\mathrm{d}\chi}{\mathrm{d}n}\mathrm{d}n = -\sqrt{\frac{2\varepsilon}{\Gamma}}\cdot f(n_{\min}) \tag{80}$$

In this equation, $f(n_{\min})$ is defined as the integral with respect to n, as shown in (81). Since $n_{\max}$ and C are dependent on $n_{\min}$, as shown in (76), this integral is only correlative with $n_{\min}$.

$$f(n_{\min}) = -\int_{n_{\max}}^{n_{\min}} \frac{\mathrm{d}n}{n\sqrt{\ln n - n + C}} \tag{81}$$

Accordingly, the period length in time could be estimated by (82). In this equation, for Ma < 10, the error caused by substituting 1 for $\sqrt{1-2k}$ is less than 8%. Hence period length in time is approximately independent on velocity. It is only decided by the minimum load factor $n_{\min}$.

$$T = \frac{T_\chi R_E}{V} = \sqrt{\frac{2\varepsilon}{1-2k}}\cdot\frac{R_E}{g}\cdot f(n_{\min}) \tag{82}$$

Supposing that $C_L = C_{Lk}$, then the period length is only decided by the maximum altitude difference ΔH. The correlation between maximum altitude difference and period length in time is plotted in Fig. 14. In the figure, the abscissa is the maximum altitude difference, and the ordinate is the period length in time. The correlation is quasi-linear and could be fitted as (83). In this figure, the altitude difference contributed by lift coefficient is neglected. Hence the estimation of period length in (82) is lower than practical, which could be observed in Fig. 14. The figure indicates that periodicity of the 2D subsystem could approximate that of the optimal PHC trajectories.

$$\tilde{T}(\mathrm{s}) = 1.7(\Delta H) + 160 \tag{83}$$

Therefore, the 2D autonomous subsystem is decided by the minimum load factor (or maximum altitude difference). This subsystem could describe the variations of normalized density (or load factor) and flight path angle with respect to normalized distance. And period length in time of an optimal PHC trajectory could be estimated by its maximum altitude difference.

B. ENERGY CYCLE

With the dynamical model of specific kinetic energy in (73) integrated, the variation of kinetic energy over one period could be obtained as

$$\int_0^{T_\chi} \dot{k}\mathrm{d}\chi = \int_0^{T_\chi} (nC_A - \gamma)\mathrm{d}\chi \tag{84}$$

With dynamical model of normalized altitude in (11) substituted, the variation in (84) could be revised as

$$\int_0^{T_\chi} \dot{k}\mathrm{d}\chi = \int_0^{T_\chi} nC_A\mathrm{d}\chi - \int_0^{T_\chi} \dot{h}\mathrm{d}\chi \tag{85}$$

According to the boundary condition of periodicity in (20), variations of kinetic energy and altitude in one period are zeros. Hence the integral of nC_A in one period is also zero, as shown in (86). The equation means that the energies supplied by propulsion and consumed by drag should balance.

$$\int_0^{T_\chi} nC_A = \frac{1}{C_L}\int_0^{T_\chi} n(C_T - C_D)\mathrm{d}\chi = 0 \tag{86}$$

As shown in Fig. 4, the scramjet tends to start at the minimum altitude. At low altitude, the vehicle boosts to ascend, and glides to descend. Since influence of propulsion is ignorable in rarefied atmosphere, it is rational to assume that the scramjet works during the whole ascending process ($\gamma > 0$) and idles during the whole descending process ($\gamma < 0$). With singularity in (48) ignored, a simplified control law of thrust coefficient is

$$C_T = \begin{cases} C_{T\max}, & \gamma > 0 \\ C_{T\min}, & \gamma < 0 \end{cases}. \tag{87}$$

According to the energy balance in (86) and the symmetry of history of normalized density in Fig. 7, this control law exactly holds in condition of (88).

$$C_{T\max} + C_{T\min} = 2C_D \tag{88}$$

With dynamical models of load factor in (70) and kinetic energy in (73) combined, the differential correlation between the two state variables could be described by (89).

$$\mathrm{d}k = \varepsilon\,(\mathrm{d}\ln n - nC_A d\chi) = -\mathrm{d}h - \varepsilon C_A\frac{\mathrm{d}n}{\gamma} \tag{89}$$

By integrating the two sides in (89), the correlation between kinetic energy and load factor could be converted into an algebraic one, as shown in (90). The physical significance of the equation is mechanical energy conservation.

$$\begin{cases} k - k(h_{\min}) = -(h - h_{\min}) - \varepsilon\int_{n_{\max}}^{n}\dfrac{C_A}{\gamma}\mathrm{d}n & (\gamma > 0) \\ k - k(h_{\max}) = -(h - h_{\max}) - \varepsilon\int_{n_{\min}}^{n}\dfrac{C_A}{\gamma}\mathrm{d}n & (\gamma < 0) \end{cases} \tag{90}$$

Let ξ denote the integration of load factor with respect to normalized distance from χ_0 to χ, as shown in (92). In physical, ξ is nonnegative.

$$\xi = \frac{1}{T_\chi}\int_{\chi_0}^{\chi} n\mathrm{d}\chi, \quad (\chi_0 \le \chi < T_\chi + \chi_0) \tag{91}$$

With the differential correlation between load factor and normalized distance in (79) substituted, ξ could be converted into an integration with respect to load factor, as shown in (92). n_0 and n is respectively the load factor at χ_0 and χ. Since flight path angle is dependent on load factor, as shown in (75), this integration is a function dependent on n and n_0.

$$\xi(n; n_0) = \mathrm{sgn}(n - n_0) \cdot \frac{1}{T_\chi}\int_{n_0}^{n} \frac{\mathrm{d}n}{|\gamma|} \tag{92}$$

According to the symmetry of $n - \gamma$ subsystem in (75), the integral ξ from the minimum altitude to the maximum should be equal to that from the maximum to the minimum, as shown in (93). For a given altitude, the sum of integration from this altitude to the minimum during descending and that from this altitude to the maximum during ascending should be equal to an integration from the minimum altitude to the maximum, as shown in (94).

$$\xi(n_{\max}; n_{\min}) = \xi(n_{\min}; n_{\max}) \tag{93}$$

$$\xi(n; n_{\max}) + \xi(n; n_{\min}) = \xi(n_{\max}; n_{\min}) \tag{94}$$

Since $\gamma = 0$ holds at maximum and minimum altitudes, variation of flight path angle is zero, and integral of dynamical model of flight path angle in (66) from the minimum altitude to the maximum should vanish, as shown in (95).

$$\gamma(h_{\min}) - \gamma(h_{\max}) = \Gamma\int_0^{T_\chi/2} (n-1)\mathrm{d}\chi = 0 \tag{95}$$

Hence $\xi(n_{\max}; n_{\min})$ could be solved to be a constant of $1/2$, as shown in (96).

$$\xi(n_{\max}; n_{\min}) = \frac{1}{T_\chi}\int_0^{T_\chi/2} n\mathrm{d}\chi = \frac{1}{T_\chi}\int_0^{T_\chi/2} \mathrm{d}\chi = \frac{1}{2} \tag{96}$$

With properties of $\xi(n; n_0)$ in (93), (94), and (96) combined, any $\xi(n; n_{\min})$ could be obtained by a $\xi(n; n_{\max})$, as shown in (97).

$$\xi(n; n_{\min}) = \frac{1}{2} - (n; n_{\max}) \tag{97}$$

With $\xi(n; n_{\max})$ simply marked as $\xi(n)$, the normalized specific kinetic energy during descending and descending could respectively be revised as (98) and (99). Values of $\xi(n)$ at different load factors are plotted in Fig. 15. The histories of kinetic energy of PHC and 1D subsystem are plotted together in Fig. 16. The figure shows that the 1D subsystem governed by (73) could describe the variation of kinetic energy well. However, this estimation is on basis of assumption that the engine starts at the minimum altitude and cutoffs at the maximum. If condition in (88) could not approximately hold, this estimation is inapplicable.

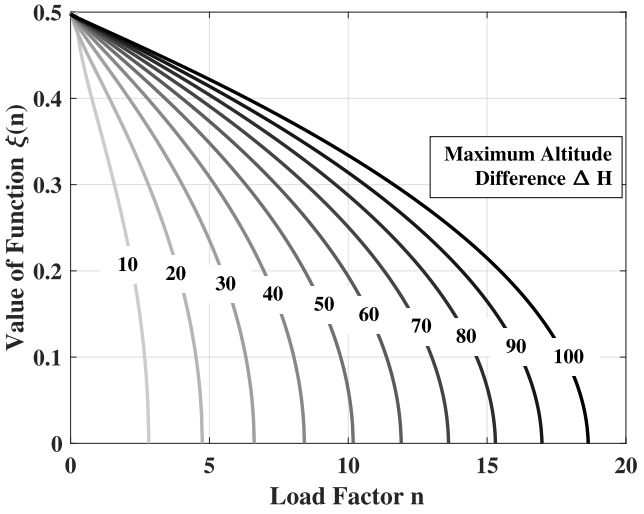

FIGURE 15. Integral of load factor with respect of χ.

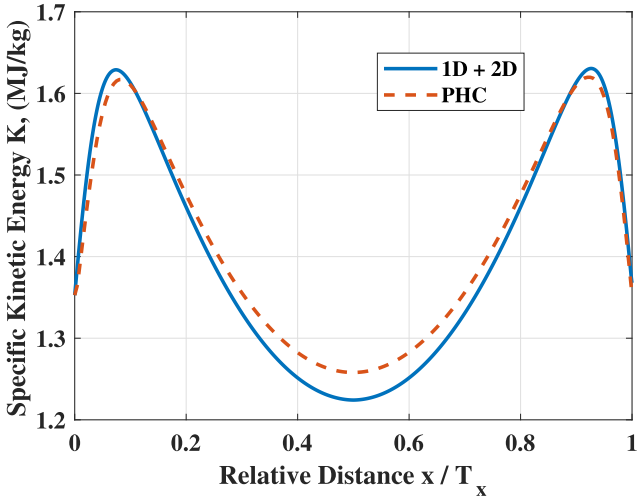

FIGURE 16. History of kinetic energy.

$$k - k(h_{\min}) = -(h - h_{\min}) + C_{A\max} T_\chi \xi(n) \tag{98}$$

$$k - k(h_{\max}) = -(h - h_{\max}) + C_{A\min} T_\chi \left[\frac{1}{2} - \xi(n)\right] \tag{99}$$

C. HEATING PERFORMANCE

According to aerothermodynamic model in (18), aerodynamic heating at stagnation point of the vehicle is a function of atmospheric density and velocity. With this model, heating performance of optimal steady cruise in (32), and definition of load factor in (65) combined, the heating performance (mean heat flux) of PHC-CL could be revised as

$$\left(\frac{\Delta Q}{T_\chi}\right)_{\text{PHC-CL}} = \dot{Q}_0\sqrt{\frac{C_{Lk}}{C_L}} \cdot \frac{1}{T_\chi}\int_0^{T_\chi} \frac{k}{k_0}\sqrt{n}\mathrm{d}\chi. \tag{100}$$

With $k \equiv k_0$ substituted into the heating performance of PHC-CL in (100), that of the 2D subsystem could be estimated by (101). According to Subsection II-B, the Mach number of optimal steady cruise is the maximum. Hence $k_0 = k_{\max}$. For PHC-CL trajectories, $k \leq k_0$. For the 2D subsystem, $k = k_0$. Hence mean heat flux of PHC is lower than the 2D subsystem.

$$\left(\frac{\Delta Q}{T_\chi}\right)_{\text{2D}} = \dot{Q}_0 \sqrt{\frac{C_{Lk}}{C_L}} \frac{1}{T_\chi} \int_0^{T_\chi} \sqrt{n} \mathrm{d}\chi \geq \left(\frac{\Delta Q}{T_\chi}\right)_{\text{PHC-CL}} \tag{101}$$

According to boundary condition of periodicity in (20), the variation of flight path angle in one period should be zero. Then the integral of dynamical model of flight path angle in (66) with respect to normalized distance in one period should vanish, as shown in (102).

$$\gamma(T_\chi) - \gamma(0) = \Gamma \int_0^{T_\chi} (n-1) \mathrm{d}\chi = 0 \tag{102}$$

Then the mean value of n in one period could be solved as 1, as shown in (103).

$$\frac{1}{T_\chi} \int_0^{T_\chi} n \mathrm{d}\chi = \frac{1}{T_\chi} \int_0^{T_\chi} \mathrm{d}\chi = 1 \tag{103}$$

And that of $\sqrt{n}$ should be less than 1, as shown in (104).

$$\frac{1}{T_\chi} \int_0^{T_\chi} \sqrt{n} \mathrm{d}\chi \leq \frac{1}{T_\chi} \int_0^{T_\chi} \frac{(n+1)}{2} \mathrm{d}\chi = 1 \tag{104}$$

With (104) substituted into heating performance of the 2D subsystem in (101), since $C_L/C_{Lk} \geq 1$, the mean heat flux of the 2D subsystem should be lower than that of steady cruise. Therefore, the mean heat flux of PHC is lower than that of steady cruise.

The mean heat flux the 2D subsystem is plotted in Fig. 17 with that of PHC. In this figure, the abscissa is the maximum altitude difference, and the ordinate is the relative aerodynamic heat flux (or the heat flux ratio of periodic to steady cruises). The blue solid curve is the heating performances of the 2D subsystem at difference altitudes, and the orange dashed one is that of PHC. The figure indicates that heating performance of the 2D subsystem matches with that of PHC. With the increment of maximum altitude difference, the mean heat flux declines. When processing the figure, lift coefficient is supposed to be C_{Lk} which is related to the maximum L/D. This assumption would lead to a higher estimation of mean heat flux than practical.

Therefore, PHC has a nature to alleviate aerodynamic heating, and its heating performance could be estimated by the performance of the 2D subsystem in (101). The mean heat flux would decline with increment of the maximum altitude difference.

D. FUEL PERFORMANCE

With the performance measure of PHC in (33), the dynamical model of fuel mass fraction in (16), and the definition of

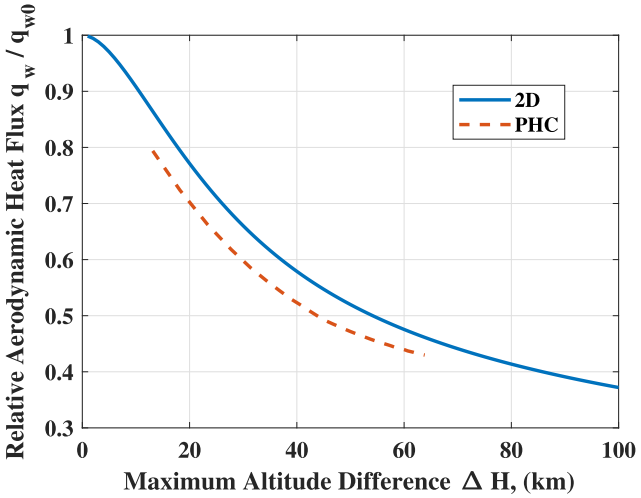

FIGURE 17. Mean heat flux of PHC and 2D autonomous system.

propulsive efficiency in (15) combined, the fuel performance of PHC could be estimated by

$$\left(\frac{\Delta \mu}{T_\chi}\right)_{\text{PHC}} = \frac{2\sigma}{h_p} \cdot \frac{1}{T_\chi} \int_0^{T_\chi} \frac{k d C_T}{\eta_P} \mathrm{d}\chi. \tag{105}$$

With $k = k_0$, energy balance condition of 1D subsystem in (86), and the equilibrium condition of flight path angle in (68) substituted, the heating performance of 2D+1D system could be estimated by (106). Since $E \leq E_{\max}$, the specific fuel consumption of 2D+1D system is not less than the optimal steady cruise. Since $C_L \geq C_{Lk}$, with increment of lift coefficient, the ratio $E_{\max}/E$ would augment. That means the fuel performance of periodic cruise would be worse. However, with the aerodynamic model in (3) considered, for $C_L/C_{Lk} \in [1, 1.33]$, the maximum ratio $E_{\max}/E$ is 1.04, which means an increment of specific fuel consumption by 4%. According to performances of PHC in Fig. 8, the maximum increment would be more than 30%. Therefore, the 1D subsystem with assumption of $k = k_0$ could not be used to estimate the fuel performance of PHC.

$$\left(\frac{\Delta \mu}{T_\chi}\right)_{\text{1D}} = \frac{1-2k}{h_p \eta_P E} = \frac{E_{\max}}{E} \dot{\mu}_0 \tag{106}$$

According to fuel performance in (105), most fuel consumption occurs at low altitude (high atmospheric density). However, Fig. 10 shows that energy conservation does not hold at low altitude. Hence the variations of flight path angle and altitude (or density) should not be decoupled from that of kinetic energy (or velocity). Then approximations of constant k, energy balance condition of 1D subsystem in (86), and the equilibrium condition of flight path angle in (68) are infeasible.

With dynamical models of kinetic energy and altitude in (11) substituted into fuel performance of PHC in (105), the fuel consumption is proportional to an integral as follows:

$$\theta = \frac{1}{T_\chi} \int_0^{T_\chi} \frac{1}{\eta_P} \left[\frac{\dot{k} + (1-2k)\dot{h}}{2\sigma} + k d C_D \right] \mathrm{d}\chi. \tag{107}$$

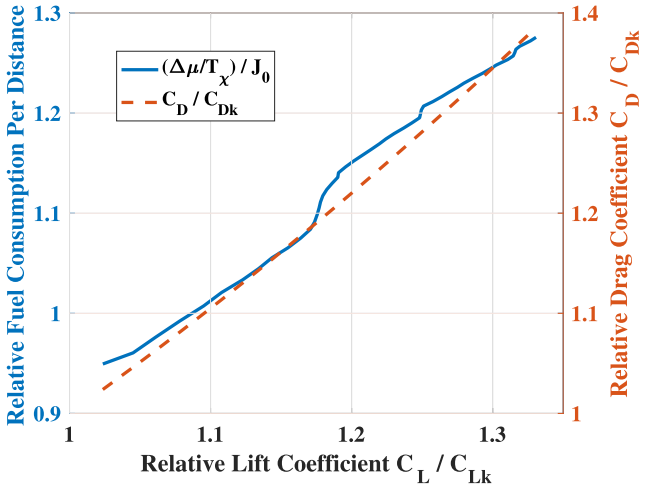

FIGURE 18. Fuel consumptions and drag coefficients at different optimal lift coefficients.

With boundary condition of periodicity in (20) substituted, with impact factor of centrifugal force $(1 - 2k)$ ignored, by mean value theorem of integrals, the function could be revised as (108). The equation indicates that the fuel consumption is proportional to drag coefficient.

$$\theta = \left(\frac{k}{\eta_P}\right)_{k=k_1} \bar{d} \cdot C_D \tag{108}$$

The ratio of PHC-CL to optimal steady cruise in fuel consumption is plotted in Fig. 18, with that in drag coefficient. The abscissa denotes that of lift coefficient. The left ordinate denotes the relative fuel consumption $(\Delta\mu/T_\chi)/J_0$, and the right one does the relative drag coefficient C_D/C_{Dk}. The figure indicates that the variation of fuel performance of periodic cruise matches with that of drag coefficient. The fuel performance of PHC could be estimated by drag coefficient, as shown in (109). The equation indicates that the impact of $\bar{d}k/\eta_P$ on fuel performance is about 10%.

$$\frac{\Delta\mu}{T_\chi} = \left(\frac{C_D}{C_{Dk}} - 0.1\right)\dot{\mu}_0 \tag{109}$$

With aerodynamic models in (3) and (31) combined, the relative drag coefficient in (109) could be substituted by a function of relative lift coefficient in (110).

$$\frac{C_D}{C_{Dk}} = \frac{1}{2}\left[1 + \left(\frac{C_L}{C_{Lk}}\right)^2\right] \tag{110}$$

Therefore, fuel performance of PHC-CL is mainly dependent on drag coefficient.

V. CONCLUSION

This work studies the trajectory features of optimal periodic control of hypersonic cruise vehicle. By this study, periodic hypersonic cruise could be realized with less technical merit of control, thus making this kind of trajectory more feasible. The features are also suggestive in further trajectory design/optimization with considerations of conserving fuel and alleviating aerodynamic heating. Besides, in preliminary designs including trajectory, the features could help to construct a routine from flight conditions to fuel and heating performances of periodic cruise. The next works will contain stability analysis of periodic hypersonic cruise trajectory, design of suboptimal stable closed-loop control law, and periodic optimal control of a PDE-ODE system with thermodynamics included.

The remarkable conclusions of this work are as follows:

1) The vehicle stays at high altitude for longer time/range.
2) Lift coefficient could be a constant and be optimized as a parameter.
3) At high altitude, dynamical models of flight path angle and altitude could be decoupled from that of velocity.
4) Period length in time is approximately irrelevant with velocity. It augments with the maximum altitude difference (a description of oscillation amplitude of altitude history) in a quasi-linear way.
5) The decoupled 2D and 1D subsystems could approximate the variations of the variables of original 3D system.
6) PHC has a nature to alleviate aerodynamic heating, and the mean heat flux would decrease with the increment of maximum altitude difference.
7) The fuel performance is mainly dependent on the constant drag coefficient.

REFERENCES

[1] J. Steelant, "Sustained hypersonic flight in europe: First technology achievements within LAPCAT II," in *Proc. 17th AIAA Int. Space Planes Hypersonic Syst. Technol. Conf.*, Apr. 2011, p. 2243, doi: 10.2514/6.2011-2243.
[2] E. Blanvillain and G. Gallic, "HIKARI: Paving the way towards high speed air transport," in *Proc. Int. Space Planes Hypersonic Syst. Technol. Conf.*, 2015, p. 3676.
[3] N. Favaloro, G. Pezzella, V. Carandente, R. Scigliano, M. Cicala, and G. Morani, "Design analysis of the high-speed experimental flight test vehicle HEXAFLY-international," in *Proc. 20th AIAA Int. Space Planes Hypersonic Syst. Technol. Conf.*, 2015, p. 3607.
[4] V. Wartemann, A. Wagner, and T. Eggers, "Passive hypersonic boundary layer control: The potential of an ultrasonically absorptive ceramic for HEXAFLY-INT," in *Proc. AIAA AVIATION Forum. Amer. Inst. Aeronaut. Astronaut.*, Jun. 2016, p. 4250, doi: 10.2514/6.2016-4250.
[5] J. Hank, J. Murphy, and R. Mutzman, "The X-51A scramjet engine flight demonstration program," in *Proc. 15th AIAA Int. Space Planes Hypersonic Syst. Technol. Conf.*, Apr. 2008, p. 2540.
[6] R. Mutzman and S. Murphy, "X-51 development: A chief engineering's perspective," in *Proc. 17th AIAA Int. Space Planes Hypersonic Syst. Technol. Conf.*, vol. 13, 2011, p. 846.
[7] D. Chai, Y.-W. Fang, Y.-L. Wu, and S.-H. Xu, "Boost-skipping trajectory optimization for air-breathing hypersonic missile," *Aerosp. Sci. Technol.*, vol. 46, pp. 506–513, Oct./Nov. 2015.
[8] H. An, C. Wang, and B. Fidan, "Sliding mode disturbance observer-enhanced adaptive control for the air-breathing hypersonic flight vehicle," *Acta Astronautica*, vol. 139, pp. 111–121, Oct. 2017. [Online]. Available: http://www.sciencedirect.com/science/article/pii/S0094576516301011
[9] S. Eyi and M. Yumuşak, "Aerothermodynamic shape optimization of hypersonic blunt bodies," *Eng. Optim.*, vol. 47, no. 7, pp. 909–926, 2015, doi: 10.1080/0305215X.2014.933822.
[10] D. Glass, "Ceramic matrix composite (CMC) thermal protection systems (TPS) and hot structures for hypersonic vehicles," in *Proc. 15th AIAA Int. Space Planes Hypersonic Syst. Technol. Conf.*, 2008, p. 2682.

[11] T.-T. Zhang, Z.-G. Wang, W. Huang, and L. Yan, "A review of parametric approaches specific to aerodynamic design process," *Acta Astronautica*, vol. 145, pp. 319–331, Apr. 2018. [Online]. Available: http://www.sciencedirect.com/science/article/pii/S0094576517319045
[12] F. Qu, D. Sun, and G. Zuo, "A study of upwind schemes on the laminar hypersonic heating predictions for the reusable space vehicle," *Acta Astronautica*, vol. 147, pp. 412–420, Jun. 2018. [Online]. Available: http://www.sciencedirect.com/science/article/pii/S0094576517316132
[13] S. Kumar and S. P. Mahulikar, "Selection of materials and design of multilayer lightweight passive thermal protection system," *J. Thermal Sci. Eng. Appl.*, vol. 8, no. 2, p. 021003, 2016.
[14] T. Kanda and T. Hiraiwa, "Evaluation of effectiveness of periodic flight by a hypersonic vehicle," *J. Aircr.*, vol. 44, no. 6, pp. 2076–2077, May 2007, doi: 10.2514/1.31143.
[15] S. Hu, C. Jiang, Z. Gao, C. Lee, and G. Zuo, "Design of periodic cruise vehicle based on the passive waverider method," in *Proc. SPACE Conf. Expo.*, Aug. 2015, p. 4546, doi: 10.2514/6.2015-4546.
[16] W. Wenkai, Z. Hou, D. Liu, J. Yang, L. Chen, and B. Zhu, "Heat-augmented trajectory optimization of hypersonic cruise vehicle," in *Proc. 21st AIAA Int. Space Planes Hypersonics Technol. Conf.*, 2017, p. 2156.
[17] L. D. Dewell and J. L. Speyer, "Fuel-optimal periodic control and regulation in constrained hypersonic flight," *J. Guid., Control, Dyn.*, vol. 20, no. 5, pp. 923–932, Jan. 1997.
[18] F. Rankins and D. J. Pines, "Relative heat load comparison of vehicles flying hypersonic transatmospheric trajectories," *J. Spacecraft Rockets*, vol. 37, no. 4, pp. 491–498, 2000.
[19] D. J. Pines, L. von Eggers Rudd, and P. H. Carter, II, "Fundamental physics of periodic hypersonic cruise trajectories," Dept. Aerosp. Eng., Univ. Maryland, College Park, MD, USA, Tech. Rep., 1998. [Online]. Available: https://www.researchgate.net/publication/2307220_Fundamental_Physics_of_Periodic_Hypersonic_Cruise_Trajectories
[20] B.-N. Kang, D. B. Spencer, S. Tang, and D. Jordan, "Optimal periodic cruise trajectories via a two-level optimization method," *J. Spacecraft Rockets*, vol. 47, no. 4, pp. 597–613, May 2010, doi: 10.2514/1.47365.
[21] W. Wenkai, H. Zhongxi, S. Shangqiu, G. Tianhao, and C. Lili, "Optimal periodic control of hypersonic cruise vehicle," in *Proc. 36th Chin. Control Conf. (CCC)*, Jul. 2017, pp. 2477–2482.
[22] P. K. Menon, G. D. Sweriduk, and A. H. Bowers, "Study of near-optimal endurance-maximizing periodic cruise trajectories," *J. Aircr.*, vol. 44, no. 2, pp. 393–398, 2007.
[23] R. T. Evans, "Optimal periodic control theory," Frank J Seiler Res. Lab, United States Air Force Acad., Colorado Springs, CO, USA, Tech. Rep. ADA093622, 1980.
[24] W. Wenkai, H. Zhongxi, S. Shangqiu, and C. Lili, "Fuel and heating performances of periodic hypersonic cruise: A mechanism analysis," in *Proc. 30th Chin. Control Decis. Conf. (CCDC)*, Jun. 2018, pp. 1609–1614.
[25] G. Masuya, T. Uemoto, Y. Wakana, K. Kudou, A. Murakami, and T. Komuro, "Performance evaluation of scramjet combustors using kinetic energy and combustion efficiencies," *J. Propuls. Power*, vol. 15, no. 3, pp. 401–407, 1999.
[26] A. Viviani and G. Pezzella, *Aerodynamic and Aerothermodynamic Analysis of Space Mission Vehicles*. Basel, Switzerland: Springer, 2015.
[27] K. Wang, B. Zhang, and Y. Hou, "Multiobjective optimization of steady-state cruise trajectory for a hypersonic vehicle," in *Proc. 3rd IEEE Int. Conf. Control Sci. Syst. Eng. (ICCSSE)*, Aug. 2017, pp. 130–135.
[28] A. Iserles, *A First Course in the Numerical Analysis of Differential Equations* (Cambridge Texts in Applied Mathematics), 2nd ed. New York, NY, USA: Cambridge Univ. Press, 2009.
[29] A. Wächter and L. T. Biegler, "On the implementation of an interior-point filter line-search algorithm for large-scale nonlinear programming," *Math. Program.*, vol. 106, pp. 25–57, Mar. 2006.
[30] A. Walther and A. Griewank, "Getting started with ADOL-C," in *Combinatorial Scientific Computing*, U. Naumann and O. Schenk, Eds. Boca Raton, FL, USA: CRC Press, 2012, pp. 181–202.
[31] D. Grass, J. P. Caulkins, G. Feichtinger, G. Tragler, and D. A. Behrens, *Optimal Control of Nonlinear Processes: With Applications in Drugs, Corruption, and Terror*. Berlin, Germany: Springer-Verlag, 2008.
[32] R. F. Hartl, S. P. Sethi, and V. G. Raymond, "A survey of the maximum principles for optimal control problems with state constraints," *SIAM Rev.*, vol. 37, no. 2, pp. 181–218, 1995.

WENKAI WANG received the B.Sc. degree in space engineering and the M.Sc. degree in aeronautical and astronautical science and technology from the National University of Defense Technology, China, in 2012 and 2014, respectively, where he is currently pursuing the Ph.D. degree in aeronautical and astronautical science and technology with the College of Aerospace Science and Engineering under the supervision of Prof. Z. Hou. He has authored or co-authored several articles in the field of aircraft design and control. His current research interests include preliminary design, flight dynamics, and optimal control for hypersonic cruise vehicles.

ZHONGXI HOU received the Ph.D. degree in computational fluid dynamics from the National University of Defense Technology (NUDT), China, in 2000. He founded the Near Space Technology Research Center, NUDT. He is currently a Professor in aeronautical and astronautical science and technology with the College of Aerospace Science and Engineering, NUDT. He has authored a monograph and over 40 international journal papers. His main research interests include aircraft conceptual design technology of high-altitude long-endurance solar-powered unmanned aircraft system, aerodynamics parameters study of aircrafts, high-resolution and high-efficient computational methods in CFD, parallel calculated methods on cluster of workstations, and massively parallel processing system with message passing interface service.

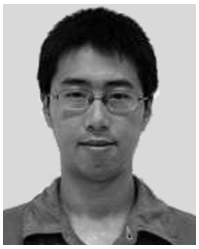

SHANGQIU SHAN received the Ph.D. degree in aeronautical and astronautical science and technology from the National University of Defense Technology, China, in 2017. He is currently a Lecturer in aeronautical and astronautical science and technology with the Department of Aerospace Science and Technology, Space Engineering University, Beijing, China. He has authored or co-authored several articles in the field of aircraft design and control. His main research interests include flight dynamics and controller design for aircraft and trajectory optimization for unmanned aerial vehicles.

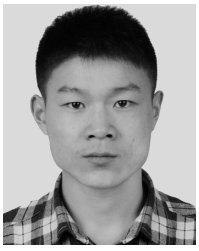

LILI CHEN received the B.Sc. degree in space engineering and the M.Sc. degree in aeronautical and astronautical science and technology from the National University of Defense Technology, China, in 2013 and 2015, respectively, where he is currently pursuing the Ph.D. degree in aeronautical and astronautical science and technology with the College of Aerospace Science and Engineering under the supervision of Prof. Z. Guo. He has authored or co-authored several articles in the field of aerodynamic design and CFD. His current research interests include aerodynamic design for hypersonic cruise vehicles.